Molecular Dynamics Simulations of Water Structure and Diffusion in a 1-nm-diameter Silica Nanopore as a Function of Surface Charge and Alkali Metal Counterion Identity

Marie Collin[a], Stéphane Gin[a,*], Baptiste Dazas[b,d], Thiruvillamalai Mahadevan[c], Jincheng Du[c], Ian C. Bourg[b]

[a] CEA Marcoule, DE2D SEVT, F-30207 Bagnols-sur-Ceze, France.

[b] Department of Civil and Environmental Engineering (CEE) and Princeton Environmental Institute (PEI), Princeton University, Princeton, New Jersey 08544, USA.

[c] Department of Materials Science and Engineering, University of North Texas, Denton, Texas 76203, USA

[d] Université de Poitiers/CNRS, UMR 7285 IC2MP, Equipe HydrASA, 5 rue Albert Turpain, Bât. B8, TSA-51106, 86073 Poitiers cedex 9, France

*Corresponding author: tel +33 466791465; fax: +33 466796620; Email address: stephane.gin@cea.fr (Stéphane Gin)

Abstract

Water confined in nanopores—particularly in pores narrower than 2 nm—displays distinct physicochemical properties that remain incompletely examined despite their importance in nanofluidics, molecular biology, geology, and materials sciences. Here, we use molecular dynamics simulations to investigate the coordination structure and mobility of water and alkali metals (Li, Na, K, Cs) inside a 1-nm-diameter cylindrical silica nanopore as a function of surface charge density, a model system particularly relevant to the alteration kinetics of silicate glasses and minerals in geologic formations. We find that the presence of negative surface charge and adsorbed counterions within the pore strongly impacts water structure and dynamics. In particular, it significantly orients water O-H bonds towards the surface and slows water diffusion by almost one order of magnitude. Ion crowding in the charged nanopore enhances the tendency of counterions to coordinate closely with the silica surface, which moderates the impact of ions on water dynamics. Co-ions are strongly excluded from the nanopore at all surface charges, suggesting that 1-nm-diameter cylindrical silica nanopores likely exhibit nearly ideal semi-permeable membrane transport properties.

Introduction

The distinct thermochemical and dynamic properties of water confined in nanopores and thin films are an important topic of study in geochemistry,[1] nanofluidics,[2] biology,[3,4] theoretical chemistry,[5,6] and materials science.[7,8] For example, nanoconfined water contributes significantly to the overall water content of many geologic materials including fine-grained (clay-rich) sedimentary rocks[9] and weathered basalt or minerals.[10,11] The impact of nanoconfinement on the transport, dielectric, and thermodynamic properties of water in these media is significant, but remains incompletely understood.[11,12]

The behavior of water in nanoconfinement is of particular interest for nuclear waste management: recent studies have shown that the long-term alteration rate of nuclear glasses in liquid water (a key parameter in predictions of nuclear waste storage security) is controlled by the formation of a nanoporous passivating layer, analogous to amorphous silica in both structure and composition, with pore diameters on the order of 1 nm.[13-15] Experimental studies suggest that a small fraction of the pore water in this layer diffuses rapidly across the layer (with an effective diffusion coefficient no more than 100 times slower than that of bulk liquid water)[15] while the remainder diffuses up to twelve orders of magnitude more slowly than bulk water (with a rate that may reflect the slow reorganization of the silica network). The diffusion of the slow water fraction shows significant sensitivity to the presence of exogenous species, in particular to the weakly-hydrated alkali metals K and Cs.[16]

Molecular dynamics (MD) simulations have played an important role in elucidating the distinct properties of nanoconfined water.[11,17] In the case of water-filled silica nanopores, most previous MD simulation studies focused on systems with uncharged pore walls with a cylindrical or slit-shaped pore geometry.[17-21] These simulations revealed that water molecules adopt a layered distribution within about 1 nm (i.e., three water monolayers) from the pore walls. In pores narrower than 2 nm, bulk-liquid-like water is absent and the sharpness of the interfacial water density layering is more pronounced. Nanoconfinement also leads to a lower

diffusivity of water molecules, with a mean diffusion coefficient roughly one order of magnitude lower than that of bulk liquid water in uncharged 1-nm-diameter pores.

The relevance to real systems of MD simulation results obtained with uncharged pores remains somewhat uncertain, because silica surfaces are well known to carry a negative proton surface charge at most pH conditions.[22] This charge originates from the silanol groups at the silica-water interface having intrinsic pK_a values of ~4 to 9 depending on their local coordination.[23-25] Glass alteration studies have been performed in a large range of pH conditions, but the alteration studies mentioned above were mostly performed in near-neutral pH conditions at 90 °C,[14,16] meaning that the pore walls likely carried a negative net proton surface charge. In these conditions, the fraction of deprotonated silanol sites on flat silica surfaces is on the order of 20 to 60 %, depending on the type electrolyte present in solution.[22,24] In silica nanopores, the fraction of deprotonated silanol sites is likely smaller because of the stronger influence of surface charge on surface electrostatic potential in confined spaces.[26,27]

To date, only a handful of MD simulation studies have examined the behavior of water in negatively charged silica nanopores.[28-32] These studies found that a charged surface leads to more hydrogen bonding between water and the silica surface, a more structured water density distribution, and a reduced water diffusivity. However, most of these studies focused on water and ion migration driven by pressure or electrostatic potential gradients[30-32] or focused primarily on systems with alkaline earth metal counterions.[28] To the best of our knowledge, no MD simulation study has yet examined the diffusion of water and ions in charged silica nanopores equilibrated with a range of alkali metal electrolyte solutions. This lack is significant, because of the important role of alkali metals as charge compensators in silicate minerals and glasses.[14,16,33-35]

The objectives of this study are, first, to gain additional insight into the extent to which water in narrow charged silica nanopores differs from bulk liquid water; second, to determine the relative importance of surface charge density and counterion type in influencing the

properties of nano-confined water and; third, to determine whether the relatively fast diffusion of a small fraction of the pore water in glass alteration layers noted above is consistent with molecular diffusion in ~1-nm-diameter charged silica nanopores. To achieve these objectives, we carried out MD simulations of water and alkali chloride ions in a 1-nm-diameter cylindrical silica nanopore developed by Bourg and Steefel [17] but modified to carry a negative surface charge density. Simulations were carried out in conditions similar to those used in recent silica glass alteration experiments (90 °C in the presence of Li-, Na-, K-, and CsCl solutions).[16] Simulations examined four surface charge densities corresponding to the deprotonation of 0 to 25 % of surface silanol groups.

Overall, our simulation results show that the self-diffusion coefficient of water in 1-nm-diameter silica nanopores is one to two orders of magnitude slower than in bulk liquid water, in agreement with the dynamics of the "fast" fraction of water in glass alteration layers observed in macroscopic experiments. Water structure and mobility in silica nanopores is sensitive to surface charge density but relatively insensitive to the identity of the alkali metal counterion, perhaps because all cations studied formed inner-sphere surface complexes at the charged silica-water interface. Simulations in which the counterions were artificially pushed away from the pore walls (to form outer-sphere surface complexes) showed a stronger impact on water structure and dynamics. Finally, MD simulations with a reactive potential suggest that water mobility is relatively insensitive to the choice of interatomic potential model.

Methods

Molecular dynamic simulations with non-reactive potentials

Molecular dynamics (MD) simulations were carried out using a modified version of the methodology of Bourg and Steefel.[17] Briefly, the simulation cell consists of a 6 nm thick amorphous silica slab pierced by a cylindrical nanopore with a radius of ~0.5 nm (Figure 1 a). The solid was created by annealing 288 unit cells of α-quartz at 5000 K, quenching to

298 K at the rate of 2 K ps^{-1}, cleaving the resulting structure to generate a nanoporous slab (i.e., removing all Si atoms located within 0.5 nm of the pore axis as well as all Si atoms located at z < 65 or z > 125 Å, then removing all O atoms that were not coordinated to at least one Si atom) and attaching an H atom to each singly-coordinated O atom to form surface silanol groups.[17] The methodology is consistent with that used in previous studies.[36] As discussed by Bourg and Steefel,[17] the resulting SiO_2 glass has an atomistic-level structure consistent with neutron diffraction experiments[37] and a low density of structural defects (0.5 % non-bridging O atoms).

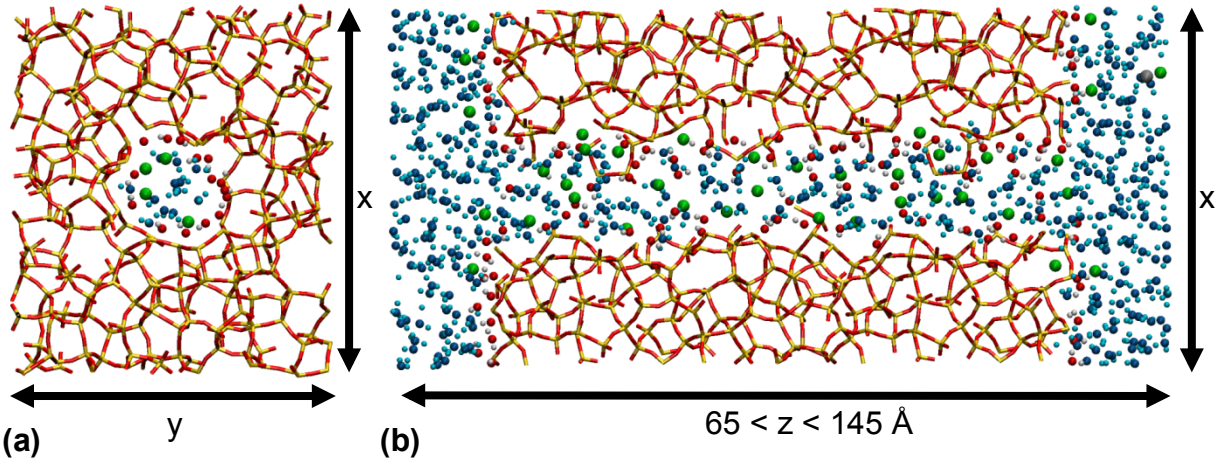

Figure 1 MD simulation snapshot showing a cross-section of the pore in directions (a) normal and (b) parallel to the pore axis. Figure b shows only the region with (65 < z < 145 Å), not the full length of the simulation cell (0 to 210 Å). Yellow, red, and white: Si, O, and H atoms in the silica structure; dark and light blue: water O and H atoms; green and grey: Cs and Cl atoms.

In order to examine the influence of surface charge density on nanoconfined water and ions, the structure used by Bourg and Steefel [17] was modified by removing 4, 10, or 25 % of surface H atoms from randomly-selected silanol groups. The largest deprotonation state is consistent with the measured net proton surface charge of silica at near neutral conditions.[24] The resulting >SiO^- functional groups were charge-balanced by addition of alkali metal counterions. Test simulations indicated that simulation results are insensitive to the starting positions of alkali metal counterions (inside or outside the pore). For simplicity, they were thus initially placed at the center of the pore or near the external surfaces of the silica slab. Water molecules were introduced in the system in quantity sufficient to fill the nanopore and form a 4 nm thick water film on each external surface of the silica slab (Figure 1 b), with the

two water films separated by a 3.4-nm-thick void gap. Finally, additional ions were introduced in each system in order to impose a background electrolyte concentration of 0.4 mol L^{-1} Li-, Na-, K-, or CsCl. The dimensions of the simulation cell are 31.65 Å x 36.54 Å x 210 Å with a total of 17 x 10^3 atoms.

Interatomic interactions were modeled using the CLAYFF model for the silica glass[38], the SPC/E model for water[39], and the parameters of Smith and Dang[40,41,42] for the alkali chloride ions (Table S1 a). Van der Waals interactions between unlike atoms were derived using the Lorentz-Berthelot combining rules. This combination of models has been successfully validated against experimental data on the structure and dynamics of bulk liquid water,[43,44] the structure of water at the quartz-water interface,[17,45] and the structure and dynamics of water on layered silicate minerals.[46-48] Water molecules were modeled as rigid bodies using the SHAKE algorithm. Silica Si and O atoms were treated as immobile atoms while silica H atoms were allowed to move in response to Coulomb, Van der Waals, and Si-O-H angle potential parameters (Table S1 a). In one simulation, denoted K25r in Table 1, an artificial repulsive force was introduced between potassium cations and silica Si atoms to assess the sensitivity of simulation results to the tendency of cations to form inner- vs. outer-sphere surface complexes (Table S1 a). Details of the simulation conditions are summarized in Table 1.

The partial charge of O atoms in deprotonated >SiO^- groups (not specified in the original CLAYFF model) was set to -1.525 e following the approach of Lammers, et al.[49] which yields CLAYFF-compatible partial charges for O atoms in silicate minerals based on their local coordination. We note that multiple approaches have been used to describe the localization of the charge arising from deprotonation of surface hydroxyl groups in previous MD simulations of Si or Ti oxide surfaces. One approach consists in simply removing the surface H atom; since hydroxyl H atoms have a partial charge of about 0.4 e in most MD simulation interatomic potential models, this yields a net charge per >SiO^- or >TiO^- group significantly lower than -1 e.[29,50] A second approach consists in distributing the remainder of the -1 e

charge beyond the deprotonated surface O atom, either up to its second-nearest neighbors[31,32,36] or over the entire surface.[51] The approach used here applies the remainder of the -1 e charge to the deprotonated O atom, an assumption consistent with other partial charges in the CLAYFF model[49] and with a subset of previous MD simulation studies of oxide surfaces.[30,52]

Each system was simulated at 348 K for durations of 1 to 9 ns, following 1 ns of equilibration, as required to characterize water diffusion into/out of the pore. Simulations were carried out in the *NVT* ensemble using a 1 fs time step. The presence of a void gap in the simulation cell effectively imposed a boundary condition $P_z = 0$ in the bulk-liquid-like water regions outside of the silica nanopore. Long-range electrostatic interactions were evaluated in reciprocal space using the particle-particle mesh (PPPM) method with a 99.99 % accuracy.[17] Temperature was controlled using a Nosé−Hoover thermostat with a coupling constant of 100 ps during equilibration and 1000 ps during simulation.[17] Simulations were carried out with the code LAMMPS[53] and the resulting data were analyzed using the code VMD[54] and in-house Matlab routines.

Molecular dynamic simulations with reactive potentials

Molecular Dynamics simulations with reactive potentials were performed to compare with the non-reactive CLAYFF simulation results. All atoms are treated through the same potential for both inter and intra molecular interactions. This allows for dissociation and reformation of complexes and also has been shown to reproduce the lifetimes of the complexes.[55] The potential has also been parameterized to show interactions in nanoconfined water in silica.[56] Specifically, the reactive MD simulations used the Mahadevan Garofalini force field (MGFF)[56,57] which allows for water dissociation and for water-glass reactions to form silanol (>SiOH) groups and siloxane (>Si-O-Si<) bridges. On the MGFF model, atomic partial charges are dynamically updated in a manner that ensures charge neutrality through the simulation. An amorphous silica block of dimensions 4 nm × 4 nm × 6 nm was created by melt-quenching a block of cristobalite with a cylindrical pore of 1 nm diameter with its axis

along the longer dimension. After surfaces were created by annealing the amorphous bloc, water molecules were added to both sides of the pore and inside the pore and allowed to interact with the glass surfaces. The simulations were carried out with the code LAMMPS[53] using tabulated potentials for the 2 body interactions and the Stillinger-Weber potentials for 3 body interactions. All the atoms were allowed to move except for small clusters of the silica block which were "frozen" to hold the silica block in place. The frozen blocks of silica were far away from the walls and water atoms and hence do not interfere in the confining regions. Simulations were carried out for at least 7.5 ns at 298 K and 348 K to compare with the simulation results obtained with the non-reactive force fields (Table 1). Figure 2 shows the arrangement of the system from two different perspectives for clarity. During equilibration, water in the pore reacts with the pore walls, forming silanol groups and also diffusing into the glass structure. Water from outside the pore enters and fills up the pore space in less than 20 ps, as seen in Figure 2 b-c.

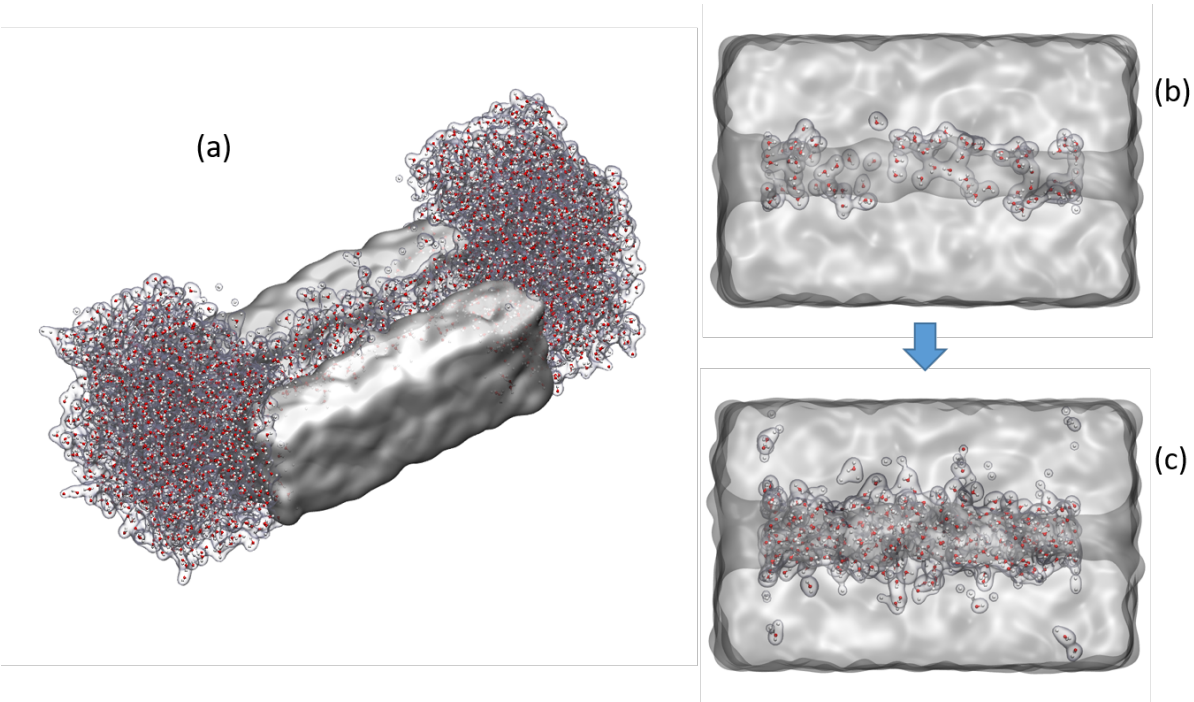

Figure 2 Snapshots of the simulations with the reactive potentials from different perspectives: (a) arrangement of the whole system with the top portion of the glass block sectioned off to show water inside the 1 nm pore; (b-c) side view after 1 ps and 5 ns of simulations showing only water molecules inside the pore. The ability of water to diffuse into the silica glass structure is evident in this view.

Data analysis

Radial distribution functions between atoms of type *i* and *j*, $g_{ij}(r)$, were determined using the code VMD.[54] The average coordination number of any atom type *i* with water oxygen atoms (O_w) was calculated from $g_{iOw}(r)$ using the following equation:

$$N_{iO_w} = 4\pi\rho_{O_w}\int_0^{r_{min}} g_{iO_w}(r)r^2\,dr \quad (1)$$

where r_{min} is the position of the first minimum of $g_{iOw}(r)$ (i.e., the boundary between the first and second solvation shells) and ρ_{Ow} is the average density of O_w atoms in the simulation cell.

Water diffusion coefficients in the pore were determined using two methodologies. First, a "local" diffusion coefficient was calculated from the mean square displacement of water O atoms [MSD(τ)] using the well-known Einstein relation:

$$D = \frac{1}{2n}\lim_{\tau\to\infty}\frac{\mathrm{dMSD}(\tau)}{\mathrm{d}\tau} \quad (2)$$

where *n* is the dimensionality of the system. Specifically, a two-dimensional map of local *D* values in axial (*z*) and radial (*r*) coordinates was calculated using Eq.(2), with *D* calculated in the direction(s) parallel to the nearest pore walls, as in Bourg and Steefel [17] The infinite time-limit in Eq.(2) was approximated using time intervals of length τ = 10 ps. The resulting map was used to calculate the average *D* value as a function of the distance from the curved surface of the nanopore (by spatially averaging the local *D* values inside the pore in the z direction) as well as the average *D* value in the entire pore (calculated as a weighted average of the local *D* values within the pore, weighted by the average number of water O_w atoms present at each coordinate).

Second, a "pore" diffusion coefficient was determined as follows: water O atoms located in the reservoirs on each side of the silica block were "tagged" after 1 ns of equilibration, while O atoms already inside the porosity were left "untagged" until they entered one of the reservoirs. The concentration of tagged water O atoms inside the pore was then monitored as a function of time. This concentration was found to increase linearly with the square root

of time in accordance with a diffusive process. The diffusion coefficient of water in the pore was determined by fitting the results to the analytical solution of Fick's second law for diffusion into a semi-infinite reservoir with boundary conditions $[O_w] = [O_w]_0$ for $z = 0$, $d[O_w]/dz = 0$ at large z, and the initial condition $[O_w] = 0$ for $z > 0$ at $t = 0$:[58]

$$[\mathrm{O_w}]_{\mathrm{pore}} = \frac{[\mathrm{O_w}]_{\mathrm{bulk\ water}}}{l} \frac{2}{\sqrt{\pi}} \sqrt{Dt} \tag{3}$$

where $[O_w]_{pore}$ and $[O_w]_{bulk\ water}$ are the concentration of tagged water O atoms in the pore and the concentration of water O atoms in bulk liquid water, respectively, and l is the pore length.

Diffusion coefficients of water molecules in the reactive MD simulations were calculated using the MSD method described above. In the reactive system, however, water and structural O atoms were not modeled as distinct chemical species, i.e., the identity of each water O atom depends dynamically on its local bonding environment. For the purpose of calculating water diffusion, water O atoms were identified as those located within 1.2 Å of at least two H atoms.

The present paper focuses particularly on the behavior of water and ions within the silica nanopore. The behavior of water and ions on the flat external surfaces of the silica slab (density profiles, etc.) is reported in the supplementary material (Fig. S2 a-l).

Cation	Name of the simulation	Temperature	Deprotonated silanol groups (%)	Surface charge density ($C \cdot m^{-2}$)	Number of cations in the system	Type of water potential	Simulation time (ns)
K	**K0**	348 K	0	0	16	Standard	10
	K4		4	0.26	26		
	K10		10	0.66	48		
	K25		25	1.65	81		
K	**K25r**	348 K	25	1.65	81	Standard	10
Li	**Li0**	348 K	0	0	16	Standard	2
	Li4		4	0.26	26		
	Li10		10	0.66	48		
	Li25		25	1.65	81		
Na	**Na0**	348 K	0	0	16	Standard	2
	Na4		4	0.26	26		
	Na10		10	0.66	48		
	Na25		25	1.65	81		
Cs	**Cs0**	348 K	0	0	16	Standard	6
	Cs4		4	0.26	26		6
	Cs10		10	0.66	48		6
	Cs25		25	1.65	81		6
-	**F348**	348 K	0	0	0	Standard	10

-	**F298**	298 K					
-	**R348**	348 K	0	0	0	Reactive	7.5
-	**R298**	298 K					

Table 1 List of the simulations carried out in this study. The K25r simulation included an artificial repulsive force between K ions and Si atoms. The last four rows describe simulations carried out with uncharged silica nanopores to determine the consistency of simulation predictions obtained with unreactive (CLAYFF+SPC/E) and reactive (GMFF) force fields.

Results and discussion

Water density distribution

Molecular dynamics simulation predictions of the impact of surface charge on water density in the nanopore are reported in Figure 3 and Figure 4 in the case of systems with K counterions. Two-dimensional maps of water O atom density (Figure 3) indicate that water molecules tend to form layers at the surface of the silica block and inside the nanopore regardless of surface charge density. This density layering extends up to ~1 nm (i.e., three water monolayers) from the silica surface, in agreement with previous studies.[17,48] In the 1 nm diameter pore, the entirety of the pore water is influenced by this density layering, suggesting that short-range interactions (e.g., steric packing and associated distortions of the hydrogen bond network) likely modulate pore water properties. This inference is consistent with previous observations indicating that confinement effects are particularly important in pores narrower than about 2 nm.[2,17]

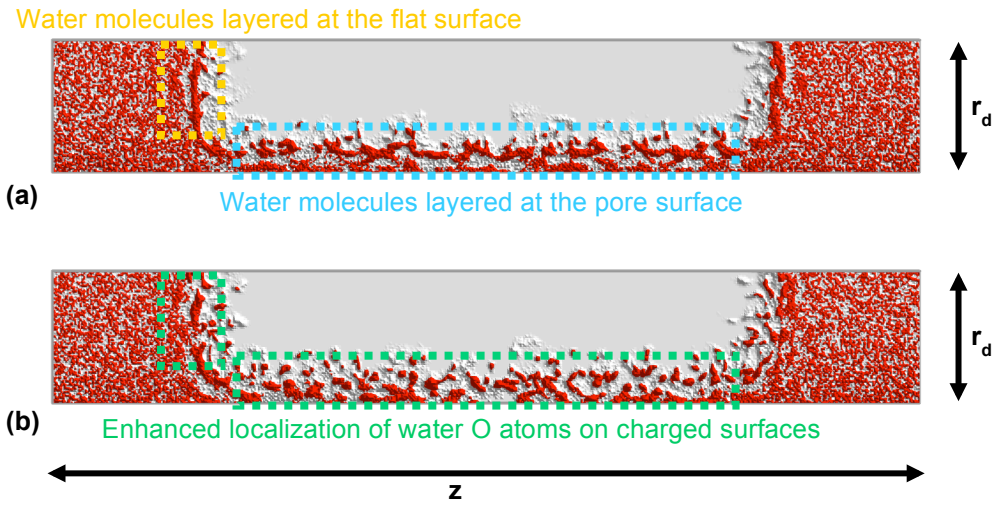

Figure 3 Average density of water O atoms (ρ_{Ow}) in pores for simulations K0 (a) and K25 (b) plotted as a function of longitudinal (z = 56−156 Å) and radial coordinates (r_d = 0.4−15 Å, i.e., distance from the pore axis). Red color indicates ρ_{Ow} values greater than the average O atoms density in the bulk liquid, white color indicates ρ_{Ow} values lower than the average value in the bulk liquid.

Comparison of predicted water density maps in uncharged and charged nanopores reveals that the presence of deprotonated silanol groups and associated counterions on the silica surface significantly enhances the localization of water O atoms within the pore and on the external surfaces of the silica slab (Figure 3). This localization likely reflects the existence of favorable sites where water molecules hydrate K ions while also donating a hydrogen bond to a $>SiO^-$ group,[28] as discussed below.

Plots of pore water O and H atom density in the radial direction (averaged over the pore length) show that surface charge has relatively little impact on the overall distribution of water O and H atoms within the pore (Figure 4). In particular, the major O_w density peaks at ~2 and ~5 Å (indicative of two layers of water molecules and of the absence of bulk-like water at the center of the pore)[17,18,21] are only weakly sensitive to surface charge (Figure 4a). The O_w density shoulder at $d \sim -1$ Å (associated with water molecules that occupy small cavities or roughness features on the silica surface)[17] increases slightly with negative surface charge density. This insensitivity to surface charge density in Figure 4a is consistent with the expectation that water O atom density distribution in the direction normal to the surface is dominated by steric effects rather than Coulomb interactions.

A greater impact of surface charge density is observed in the water H density profile (Figure 4b), where density shifts reveal a reorientation of water H atoms towards the silica surface. This reorientation also is obvious in the radial distribution functions between water H atoms (H_w) and O atoms in deprotonated silanol groups (O_d), protonated silanol groups (O_h), and water molecules (O_w) (Figure 4d). In particular, the $g(r)$ functions indicate that O_d atoms receive two to three times as many hydrogen bonds from water as do O_w or O_h atoms (nearest-neighbor O-H coordination numbers calculated with Eq. 1 equal 3.0, 1.6, and 0.8 for O_d, O_w, and O_h atoms, respectively). The $g(r)$ functions further suggest that water donates stronger hydrogen bonds to O_d atoms than to O_w or O_h atoms based on the closer position of the first peak for O_d (1.55 Å) than for O_w or O_h atoms (1.75 Å). In short, silanol group deprotonation strongly enhances the tendency of water molecules to orient their hydrogen

atoms towards the silica surface. Overall, roughly 8 (K4) to 35% (K25) of the hydrogen from water molecules confined in the pore are coordinated to deprotonated silanols. This finding is consistent with observations of interfacial water dipole reorientation on deprotonated silica[29] and other charged surfaces.[11,47,59]

Ion distribution and coordination in the nanopore

Alkali metals in our simulations show a density layering at the surface of the pore and on the flat silica surface, as illustrated in the case of potassium in Figure 4 c. In all cases, the main cation density peak is located closer to the surface than the first O_w density peak, indicating that alkali metals form inner-sphere surface complexes at the charged silica-water interface. This finding is consistent with previous MD and density function theory simulations of alkali metal interaction with uncharged and charged planar silica-water interfaces.[60]

As surface charge density increases, the main cation density peak shifts closer to the surface of the pore (from 2.10 to 1.20 Å in the case of potassium, Figure 4 c) as previously observed in simulations of charged carbon-water interfaces.[8] This closer approach to the surface results in a decrease in the aqueous coordination number of all alkali metals with increasing surface charge density, particularly within the nanopores, but also (to a smaller extent) on the external flat silica surface (Table 2). The existence of this effect on the flat silica surfaces suggests that it reflects, at least in part, the interaction of cations with multiple deprotonated silanol groups at higher surface charge densities. The enhanced effect observed in silica nanopores suggests that ion-ion repulsion within the pore may also play a significant role by "pushing" the counterions towards the surface, in agreement with studies of biological nanopores.[61] We note, in passing, that this finding contradicts the routine assumption in models of adsorption and colloidal interactions that rely on the Gouy-Chapman model of the electrical double layer that the distance of closest approach of ions to a charged surface is invariant with surface charge density.

Other impacts of adsorption or confinement on the coordination of alkali metals are more subtle. For example, the position of the $g_{C\text{-}Ow}(r)$ first peak (where C is the alkali metal cation) is similar in bulk water, near the flat surface, and inside the pore. By contrast, the $g_{C\text{-}Hw}(r)$ first peak is less sharp inside the pore and near the flat surface than in bulk water (Table S4), particularly at high surface charge densities. This indicates that the silica surface disrupts the orientation of a significant fraction of the water molecules in the first solvation shell of cations, perhaps because these water molecules adjust their orientation to coordinate withsurface silanol groups. This finding suggests that ions may be more weakly solvated in silica nanopores than in bulk liquid water, in agreement with results obtained in carbon nanotubes[7] and in clay interlayer nanopores.[62]

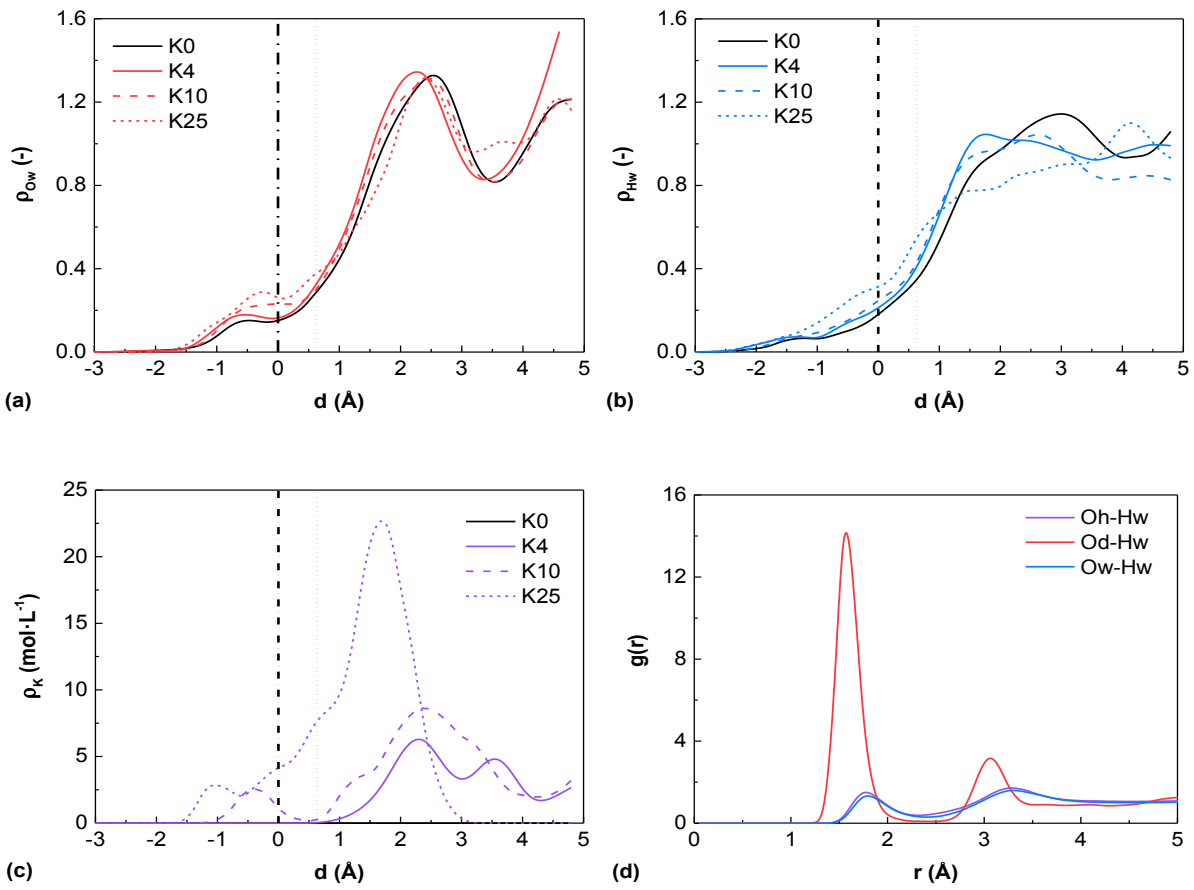

Figure 4 (a) Average density of water O atoms ρ_{Ow}, (b) water H atoms ρ_{Hw} (relative to their concentration in bulk liquid water), and (c) K atoms ρ_K (in mol L^{-1}) calculated for z = 85−125 Å as a function of the distance from the curved surface of the nanopores. The pore axis is located at d = 5 Å. The black dash-dot line at d = 0 Å delineates the region beyond which Si atoms were removed while creating the pore. The black dot line corresponds to the Gibbs surface of water as determined by Bourg and Steefel [17] in the case of the uncharged nanopore. No K atoms entered the pore during the K0 simulation run. (d) Radial distribution functions between water H atoms (Hw) and O atoms from protonated silanols (Oh), deprotonated silanols (Od), or water molecules (Ow) in simulation K10 (other data are in supplementary material Fig. S4 j-k).

	N_{H2O}		
	Bulk	**Flat**	**Pore**
K0	6.4	-	-
K4	6.2	5.5	5.5
K10	6.5	6.2	4.4
K25	6.4	4.9	3.8
K25r	7.1	7.8	5.2
Li10	4.1	2.9	2.4
Na10	5.3	4.2	3.0
Cs10	7.8	7.4	4.7

Table 2 Average number of water molecules in the first hydration shell of the cations in bulk liquid water, on the external flat silica surface, and in the nanopore calculated using Eq. 1. The relevant *g*(*r*) functions are displayed in the supplementary material (Fig. S4 a-h).

Similar results on water and ion coordination were obtained regardless of the nature of the alkali metal, with an effect on water density distribution that is minimal (Figure 5 a-b). Despite differences in cation size, the same number of each cation is found inside the pore for a given surface charge density (Figure 5 d). This is required from charge balance considerations, because anions were completely excluded from the nanopore in all simulations. Differences in coordination between the different cations are relatively minor. All cations tend to form inner sphere surface complexes at the silica-water interface, as noted above (Figure 5 c) and as attested by their aqueous coordination numbers (Table 2). Smaller alkali metals (Li, Na) tend to approach the surface more closely relative to the larger metals (K, Cs) as expected from their smaller ionic radius, in agreement with previous studies of systems where alkali metals form inner-sphere surface complexes.[63,64]

Water content in the nanopore

The average number of water molecules present in the nanopore is remarkably sensitive to surface charge density and the identity of the exchangeable cation. Overall, water content increases with surface charge, but this effect is strongly inhibited in the presence of K or Cs (Figure 5 e). This inhibition of water uptake by K and Cs likely reflects both the larger size and lower hydration energy of the larger alkali metals; for example, Cs occupies up to 30 % of the pore space in our simulations, leaving less space for water molecules. This dependence of pore water content on both surface charge density and the hydration energy of the adsorbed cation is consistent with well-known trends in water uptake by other nanoporous media including swelling clay minerals.[33,35] A rough estimate of the fraction of

nanopore water located in the first hydration shell of the cations (calculated by multiplying the average number of cations in the pore by their average aqueous coordination number and dividing by the total pore water content) suggests that the pore contains little or no “free” water at the highest deprotonation state, particularly in the presence of K or Cs (Figure 5 f). This negative influence of K and Cs on the hygroscopicity of silica nanopores is reminiscent of the tendency of K and Cs to inhibit the migration kinetics of the “slow” water fraction in hydrated amorphous silica layers (as noted in the introduction). This coincidence may hint at a possible influence of counterion hydration on the reorganization dynamics of the polymeric silica network (i.e., the presence of more weakly hydrated cations may lead to a less hydrated, less labile silica network).

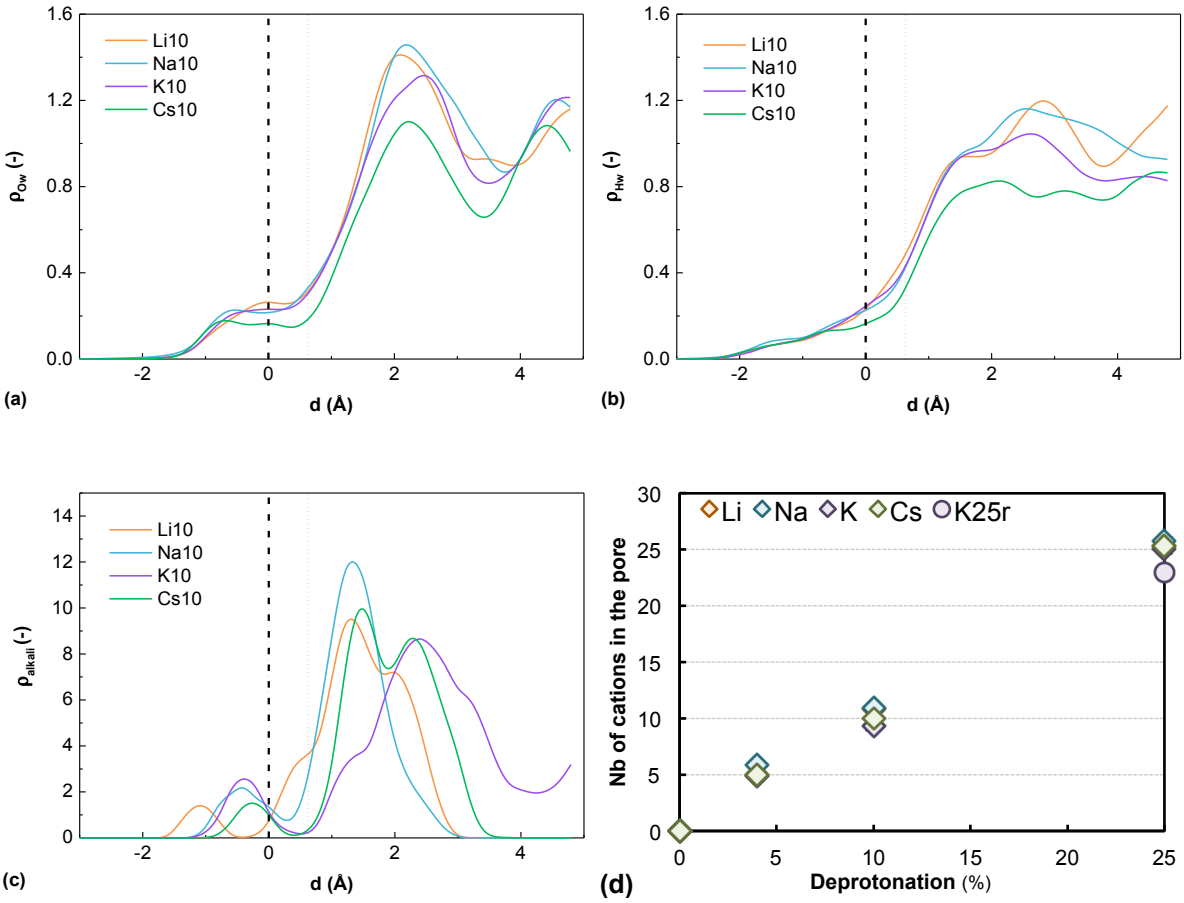

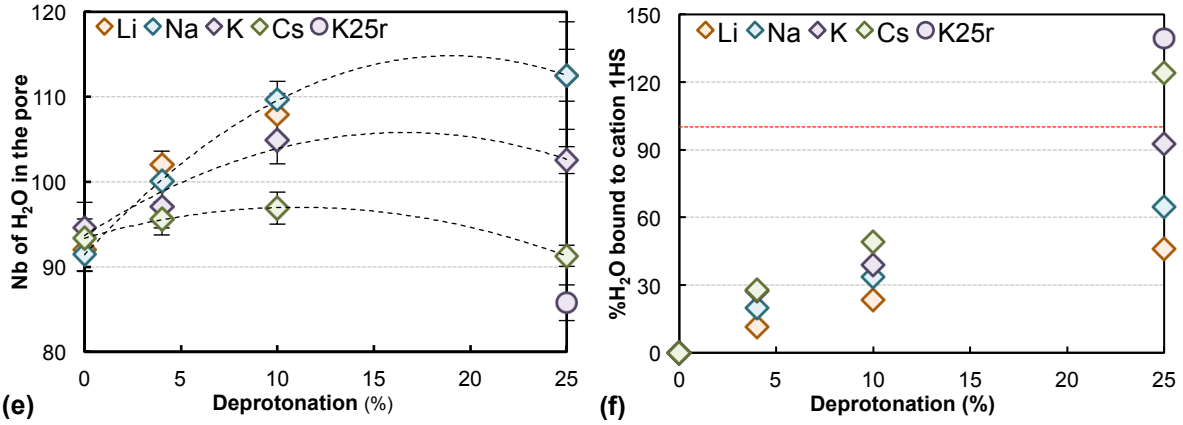

Figure 5 (a) Average density of water O atoms ρ_{Ow}, (b) water H atoms ρ_{Hw}, and (c) alkali atoms ρ_{alkali} as a function of the distance from the curved surface of the nanopores, calculated for z = 85−125 Å for each alkali metal at 10 % deprotonation. (d) Number of cations in the pore (the uncertainty bars are smaller than the symbols), (e) number of water molecules in the pore (Li and Na last points are superimposed; dashed lines are drawn to guide the eye), and (f) rough estimate of the percentage of water molecules in the pore that coordinate adsorbed cations.

Impact of cation adsorption as inner- vs. outer-sphere surface complexes

To assess the effect of the formation of inner-sphere surface complexes on water density distribution, the simulation with K at the highest surface charge density was replicated with an artificial repulsive force between K and the silica block (simulation K25r). Adsorbed cations were thus forced to form outer-sphere complexes. Interestingly, the water content of the nanopore decreases by 16 % as the ions are forced to detach from the pore surface (Figure 5 e). This decrease in water content results primarily from a decrease in water density near the pore axis (Figure 6 a-b). In short, the forced detachment of K ions from the pore walls strongly disrupts the ability of water molecules to fill the pore, even though the K ions adopt a more ordered hydration shell (Figure 6 d) and are not located on the pore axis (Figure 6 c).

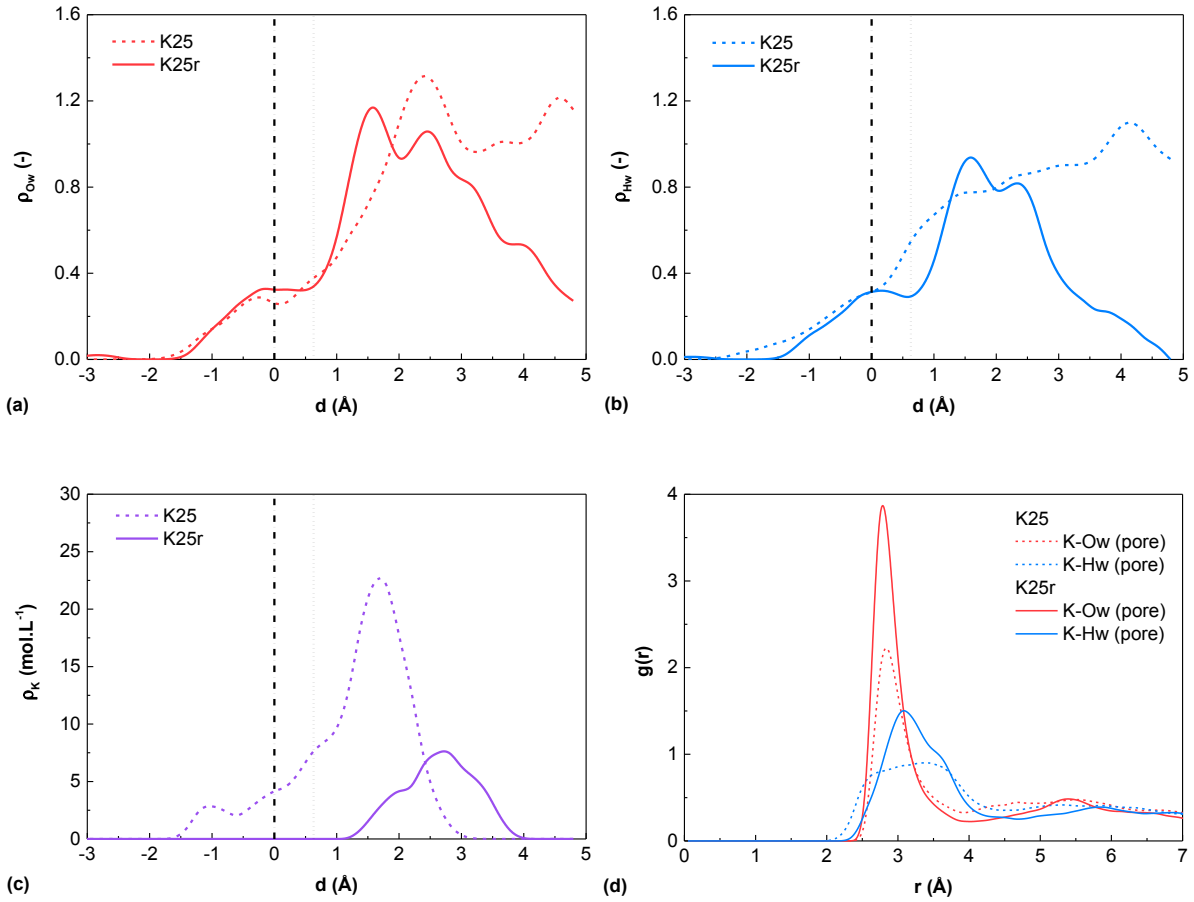

Figure 6 (a) Average density of water O atoms ρ_{Ow}, (b) water H atoms ρ_{Hw}, and (c) K atoms ρ_K as a function of the distance from the curved surface of the nanopores, calculated for z = 85−125 Å. (d) K-Ow and K-Hw Radial distribution comparison. Note that the *g(r)* does not tend to 1 as it was not corrected to take into account the excluded volume.

Salt exclusion from uncharged nanopores

In the case of the non-deprotonated system, despite simulation times longer than 10 ns, neither cations nor anions entered the pore. Longer simulations would be required to determine whether this observation reflects a kinetic or a thermodynamic limitation to the entry of ions in the nanopore. A kinetic origin is suggested by the absence of ion exchange between bulk and nanopore water in the simulations with charged pore walls during simulation runs of up to 10 ns. However, a thermodynamic origin would be expected based on both mean-field theories (because silica has a lower dielectric constant than liquid water)[65,66] and atomistic-level considerations (because nano-confinement disrupts the ability of water to solvate ions, as noted above)[62] and would be consistent with the partial or total salt exclusion observed in carbon nanotubes[8] and uncharged clay interlayer nanopores.[59]

Water and ion diffusion in the silica nanopore

Simulation results on the diffusion coefficients of O_w atoms and cations in bulk liquid water and confined water are reported in Table 3 and Figure 7. As noted in the methods section, diffusion coefficients were determined using two methods: from the slope of MSD vs. time over 10 ps and from the diffusion of "tagged" water molecules from the external water reservoirs into the nanopore. Simulation predictions of MSD vs. time had a coefficient of determination (r^2 value) near 1 for water in bulk liquid water. In the nanopore, lower r^2 values were obtained, suggesting that *D* values calculated with the MSD method may have a significantly lower precision (supplementary material Fig.S3 a-e). Nonetheless, the progressive uptake of "tagged" water in the nanopores increased linearly with the square root of time, as expected for a diffusive process (Figure 7 b), and the "tagged" water and MSD methods yielded mutually consistent *D* values for nanopore water in most cases (Table 3), which provides confidence in the accuracy of both methods.

As expected, maps of the local water *D* values in the nanopore as calculated with the MSD method indicate that water diffusivity increases with distance from the pore walls (Figure 7 a). With increasing negative surface charge density, water diffusion is inhibited roughly evenly throughout the pore. For example, in simulations with potassium counterions the water *D* value at the center of the pore decreases by a factor of 3 (from 1.5 to 0.5 × 10^{-9} $m^2 \cdot s^{-1}$) with increasing surface charge density (Figure 7 a); simultaneously, the average water diffusion coefficient in the pore also decreases by a factor of 3 (from 0.7 to 0.2 × 10^{-9} $m^2 \cdot s^{-1}$) (Figure 7 f). This slowing down of water diffusion with increasing surface charge is consistent with the structural features described above, in particular the tendency of water molecules to form strong hydrogen bonds with deprotonated silanol groups and the fact that at high surface charge densities much of the nanopore water belongs to the first hydration shells of counterions (Figure 5 f).

The identity of the exchangeable cation has remarkably little influence on water diffusion in the nanopore (Figure 7 f). The influence of cation adsorption as inner- vs. outer-sphere

surface complexes, however, may strongly influence water diffusion, though the results are ambiguous because of a large discrepancy between the two methods of quantifying water diffusion in simulation K25r (supplementary material Fig.3 d-e). The MSD method suggests that the average diffusion coefficient of nanopore water in simulation K25r was lower than in simulation K25 by a factor of ~5 (Table 3), particularly because of a very slow diffusion of water near the pore axis (Figure 7 c). This prediction is at least qualitatively consistent with experimental observations of water dynamics in Vycor glass, where the diffusion coefficient dropped by 80 % when Ca ions (which have a greater tendency to form outer-sphere surface complexes) were introduced in solution.[67]

Finally, alkali metals are predicted to diffuse up to two orders of magnitude more slowly in the nanopore than in bulk liquid water, as shown in the case of potassium in Table 3. Simulation predictions suggest that about half of this effect is caused by confinement (i.e., the *D* value of potassium decreases by one order of magnitude when going from bulk liquid water to the charged silica nanopore with the lowest charge density) while the other half is caused by ion crowding in the pore (i.e., the *D* value of potassium decreases by almost one more order of magnitude as surface charge density increases).

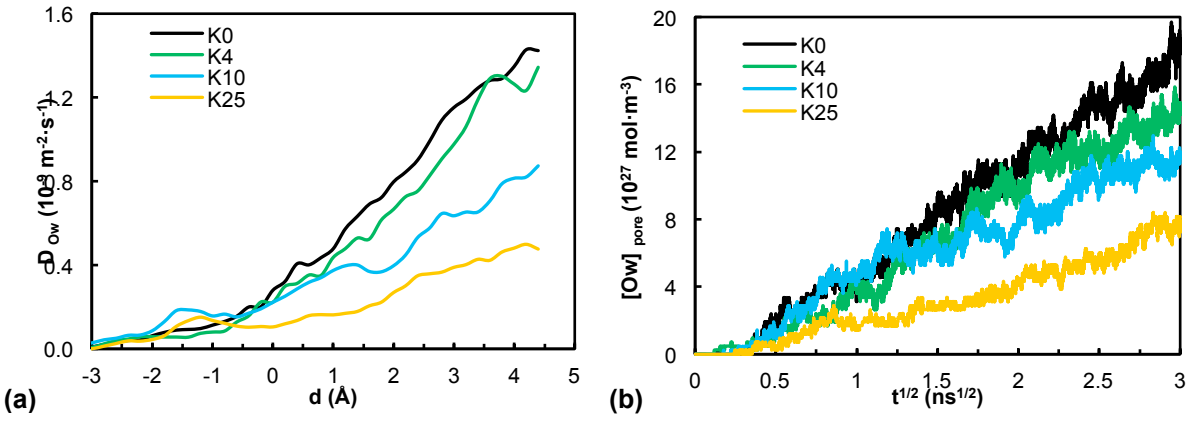

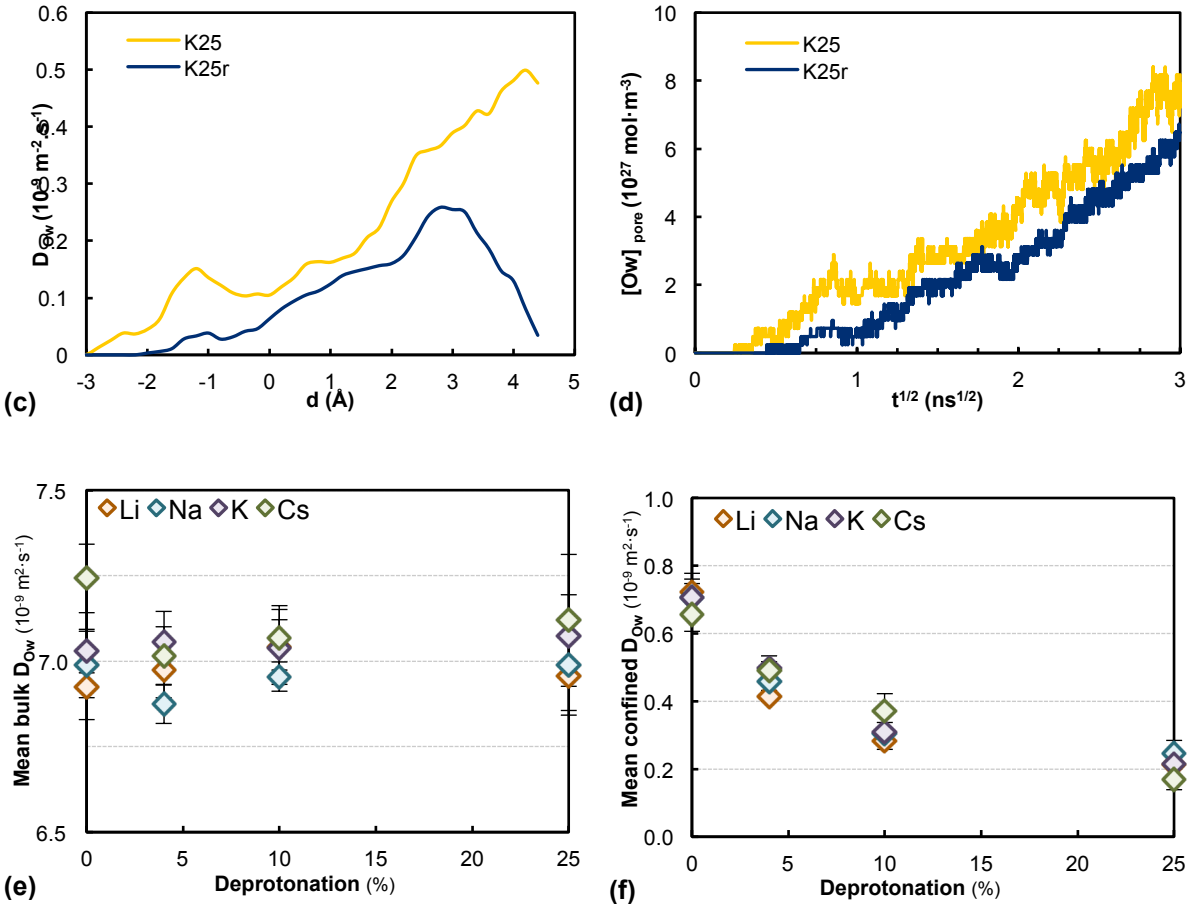

Figure 7 (a) Diffusion coefficient of O_w atoms as a function of the distance from the curved surface of the nanopore. (b) Concentration of "tagged" O_w atoms inside the pore as a function of the square-root of time (averaged over both directions). (c) Same as Fig. 7a in the case of simulations with and without the artificial repulsion between K atoms and the silica surface. (d) Same as Fig. 7b in the case of simulations with and without the artificial repulsion between K atoms and the silica surface. (e) Average *D* values of O_w in bulk water calculated with the MSD method. (f) Same as Fig. 7e in the case of nanopore water.

	$^{Bulk}D_K$ (MSD)	$^{Confined}D_K$ (MSD)	$^{Bulk}D_{Ow}$ (MSD)	$^{Confined}D_{Ow}$ (MSD)	$^{Confined}D_{Ow}$ (Ow tagged)
	(10^{-9} m^2·s^{-1})	(10^{-9} m^2·s^{-1})	(10^{-9} m^2·s^{-1})	(10^{-9} m^2·s^{-1})	(10^{-9} m^2·s^{-1})
K0	1.13 ± 0.41	-	7.03 ± 0.06	0.71 ± 0.04	0.73
K4	1.17 ± 0.44	0.08 ± 0.02	7.05 ± 0.09	0.50 ± 0.04	0.53
K10	1.24 ± 0.52	0.03 ± 0.01	7.04 ± 0.08	0.31 ± 0.03	0.26
K25	1.20 ± 0.48	0.03 ± 0.01	7.07 ± 0.12	0.21 ± 0.04	0.14
K25r	1.15 ± 0.43	0.01 ± 0.002	7.09 ± 0.07	0.04 ± 0.01	0.11

Table 3 Average diffusion coefficients of cations and water molecules in bulk water and confined water predicted with the MSD and tagged water methods.

Comparison of non-reactive and reactive simulation potentials

Water O and H density profiles obtained with both reactive and non-reactive potential at 298 and 348 K are displayed in Figure 8 a-d. The reactive potentials allow for the dissociation of water molecules and the formation of silanol groups.[68] We note that the pore diameter is slightly greater (by ~0.2 nm) in the reactive systems than in the non-reactive system because

of differences in the methodologies used to construct the simulated systems. Nevertheless, the two types of interatomic potential models yield broadly consistent results. In the simulations with reactive potentials, a small number of water molecules penetrate deeply (> 0.3 nm) into the silica structure (Figure 8 c-d) as observed in previous studies.[68] In the case of non-reactive potentials, water does not penetrate deeply into the silica structure, and water within the pore tends to exhibit somewhat sharper density peaks (Figure 8 a-b). [17,69-72] Nevertheless, the two methodologies yield similar water density layering (Figure 8 a-d) and O-H radial distribution functions (Figure 8 e-f). A shift towards a more uniform density is observed at higher temperature with both the potentials studied, though the layering still persists.

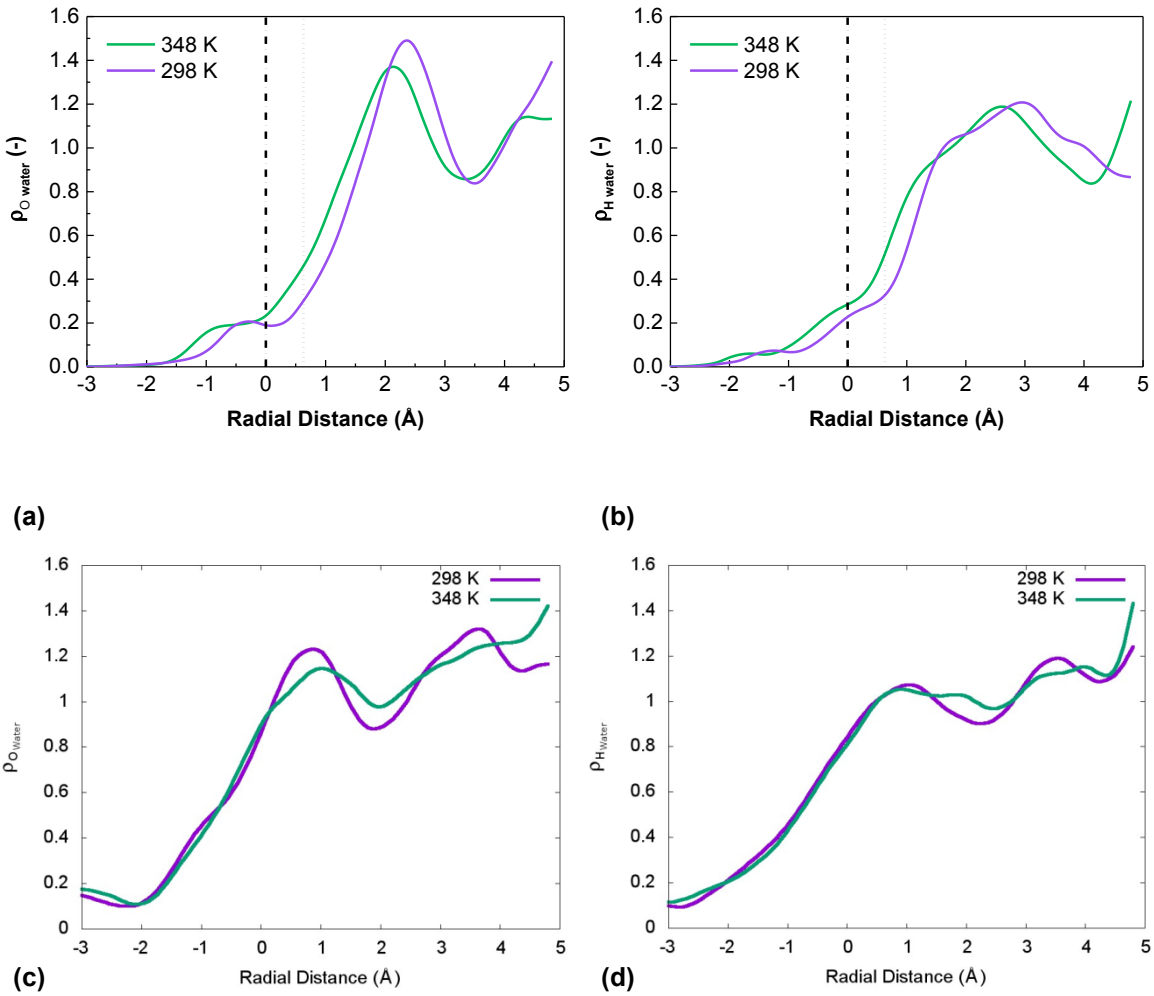

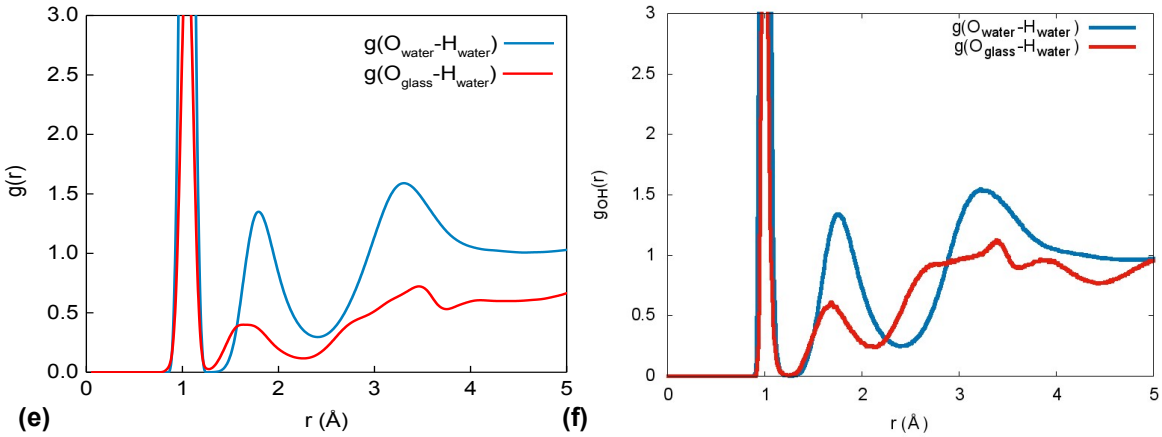

Figure 8 Radial density profiles at 298 and 348 K of (a) H and (b) O from water molecules with the non-reactive potentials and (c) H and (d) O from water molecules the reactive potentials. The data indicates a deeper penetration of water into the silica structure and persistent layering at both the temperatures. Pair distribution function between hydrogens in water and different types of oxygens in the system at 348 K. (e) Non-reactive system. (f) Reactive system, where water oxygens were isolated based on the number of their hydrogen neighbors. In both cases, the shorter distance of the $g_{Og\text{-}Hw}(r)$ second peak (~1.65 Å) compared to that of $g_{Ow\text{-}Hw}(r)$ (~1.75 Å) indicates stronger bonds between these species.

Figure 9 a-b shows a plot of the diffusion coefficient of water for two temperatures with both potentials (reactive and non-reactive). Increased temperature allows for faster diffusion of water. The highest self-diffusion coefficients, which are attained at the center of the pore (~0.5 × 10^{-9} $m^2 \cdot s^{-1}$ at 298 K, ~1.5 × 10^{-9} $m^2 \cdot s^{-1}$ at 348 K), are clearly lower than in bulk water at the same temperatures.[4,5] Overall, qualitatively consistent diffusion trends are observed with both type of inter-atomic potential models: water diffusion is similarly reduced near the pore walls in both cases, as expected because both methods yield consistent results on the coordination of hydrogen bonds with water and silica O atoms (Figure 8 e-f). The slightly faster water diffusion observed with the reactive potential is qualitatively consistent with the small difference in pore diameter between the two systems.

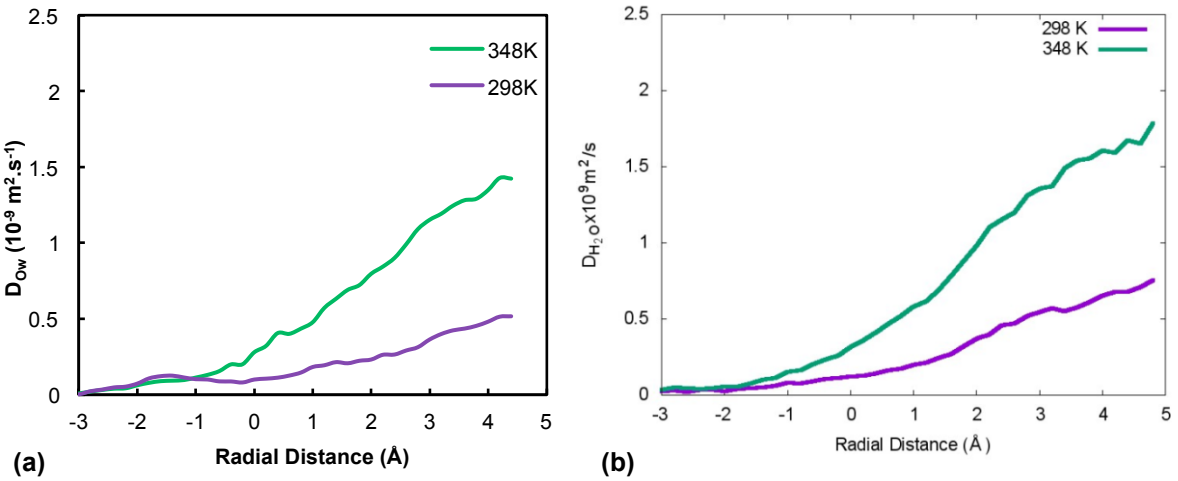

Figure 9 Diffusion coefficient of water at the two temperatures studied with (a) the non-reactive potentials and (b) with the reactive potentials. All indicate that the diffusivity of water is reduced inside the pore.

Ideally, comparative simulations of water diffusion in ion containing solutions would provide further comparison with the CLAYFF simulations. However, there are no parameters yet for alkali ions. The development of these potentials would allow detailed comparison with reactive potential simulations.

Conclusions

Overall, our simulation results reveal a significant effect of surface charge on water structure and dynamics. Water molecules form strong hydrogen bonds with deprotonated silanol groups. A large fraction of the pore water molecules solvate alkali metal counterions, but the solvation structures are disrupted by nano-confinement. The mean self-diffusion coefficient of water inside the pore is at least one order of magnitude lower than in bulk liquid water and decreases further with increasing surface charge density.

The structure of confined water is only weakly dependent of the nature of the alkali metal cation, perhaps because all metals form inner-sphere surface complexes in our simulations. The type of metal, however, significantly influences the amount of water in the pore, with larger, less hydrophilic metals (K, Cs) resulting in significantly lower pore water contents.

Finally, mutually consistent results were obtained with reactive and non-reactive interatomic potential models, though the comparison is only qualitative because of a small difference in

pore size. MD simulations with a reactive potential showed that the reorganization of the silica network (thought to govern the slow water dynamics seen in recent experimental studies)[15] occurs much more slowly than the time scale of the present simulations, as the diffusion coefficients obtained here are more than 12 order of magnitude higher than those calculated in the study of Gin et al. [15]

Supporting information

Details of our simulations, flat surface supplementary data, water diffusion supplementary data, and radial distribution function supplementary data. This material is available free of charge via the Internet at http://pubs.acs.org.

Acknowledgments

M.C., S.G., T.M. and J.D. were supported as part of the Center for Performance and Design of Nuclear Waste Forms and Containers, an Energy Frontier Research Center funded by the U.S. Department of Energy, Office of Science, Basic Energy Sciences under Award # DE-SC0016584. I.B. was supported by the U.S. Department of Energy, Office of Science, Office of Basic Energy Sciences under Award # DE-SC0018419. B.D. was partially supported by the U.S. Department of Energy, Office of Science, Office of Basic Energy Sciences under Award # DE-SC0018419, and by the CNRS interdisciplinary “défi Needs” through its “MiPor” program (Projet TRANSREAC). M.C. performed non-reactive MD simulations and wrote the paper. I.B. and B.D. were deeply involved in data interpretation. T.M. and J.D performed reactive MD simulations. S.G. supervised the study. All the authors helped on paper editing.

References

1 Bui, T., Phan, A., Cole, D. R., Striolo, A. Transport Mechanism of Guest Methane in Water-Filled Nanopores. *J. Phys. Chem. C* **2017**, *121*, 15675-15686.

2 Bocquet, L., Charlaix, E. Nanofluidics, from Bulk to Interfaces. *Chem Soc Rev* **2010**, *39*, 1073-1095.

3 Agre, P., Preston, G. M., Smith, B. L., Jung, J. S., Raina, S., Moon, C., Guggino, W. B., Nielsen, S. Aquaporin Chip: The Archetypal Molecular Water Channel. *Am. J. Physiol.* **1993**, *265*, 463-476.

4 Agre, P., King, L. S., Yasui, M., Guggino, W. B., Ottersen, O. P., Fujiyoshi, Y., Engel, A., Nielsen, S. Aquaporin Water Channels - from Atomic Structure to Clinical Medicine. *J. Physiol.* **2002**, *542*, 3-16.
5 Giovambattista, N., Rossky, P. J., Debenedetti, P. G. Computational Studies of Pressure, Temperature, and Surface Effects on the Structure and Thermodynamics of Confined Water. *Annu. Rev. Phys. Chem.* **2012**, *63*, 179-200.
6 Perkin, S., Goldberg, R., Chai, L., Kampf, N., Klein, J. Dynamic Properties of Confined Hydration Layers. *Farad. Disc.* **2008**, *141*, 399-413.
7 Shao, Q., Huang, L., Zhou, J., Lu, L., Zhang, L., Lu, X., Jiang, S., Gubbins, K. E., Shen, W. Molecular Simulation Study of Temperature Effect on Ionic Hydration in Carbon Nanotubes. *Phys. Chem. Chem. Phys.* **2008**, *10*, 1896-1906.
8 Kalluri, R. K., Konatham, D., Striolo, A. Aqueous Nacl Solutions within Charged Carbon-Slit Pores: Partition Coefficients and Density Distributions from Molecular Dynamics Simulations. *J. Phys. Chem. C* **2011**, *115*, 13786-13795.
9 Keller, L. M., Schuetz, P., Erni, R., Rossell, M. D., Lucas, F., Gasser, P., Holzer, L. Characterization of Multi-Scale Microstructural Features in Opalinus Clay. *Microp. Mesopor. Mat.* **2013**, *170*, 83-94.
10 Maher, K., Johnson, N. C., Jackson, A., Lammers, L. N., Torchinsky, A. B., Weaver, K. L., Bird, D. K., Brown, G. E. A Spatially Resolved Surface Kinetic Model for Forsterite Dissolution. *Geochim. Cosmochim. Acta* **2016**, *174*, 313-334.
11 Wang, Y. Nanogeochemistry: Nanostructures, Emergent Properties and Their Control on Geochemical Reactions and Mass Transfers. *Chem. Geol.* **2014**, *378-379*, 1-23.
12 Rotenberg, B., Cadène, A., Dufreche, J. F., Durand-Vidal, S., Badot, J. C., Turq, P. An Analytical Model for Probing Ion Dynamics in Clays with Broadban Dielectric Spectroscopy. *J. Phys. Chem. B* **2005**, *109*, 15548-15557.
13 Gin, S., Jollivet, P., Fournier, M., Angeli, F., Frugier, P., Charpentier, T. Origin and Consequences of Silicate Glass Passivation by Surface Layers. *Nat. Commun.* **2015**, *6*.
14 Collin, M., Fournier, M., Frugier, P., Charpentier, T., Moskura, M., Deng, L., Mengguo, R., Du, J., Gin, S. Structure of International Simple Glass and Properties of Passivating Layer Formed in Circumneutral Ph Conditions. *npj Mater. Degrad.* **2018**, *2*, 4.
15 Gin, S., Collin, M., Jollivet, J.-P., Fournier, M., Dupuy, L., Mahadevan, T. S., Du, J., Kerisit, S. Dynamics of Self-Reorganization Explains Passivation of Silicate Glasses *Nat. Commun.* **2018**, *In Press*.
16 Collin, M., Fournier, M., Charpentier, T., Moskura, M., Gin, S. Impact of Alkali on the Passivation of Silicate Glass. *npj Mater. Degrad.* **2018**, *2*, 16.
17 Bourg, I. C., Steefel, C. I. Molecular Dynamics Simulations of Water Structure and Diffusion in Silica Nanopores. *J. Phys. Chem. C* **2012**, *116*, 11556-11564.
18 Bonnaud, P. A., Coasne, B., Pellenq, R. J. Molecular Simulation of Water Confined in Nanoporous Silica. *J. Phys. Condens. Matter.* **2010**, *22*, 284110.
19 Siboulet, B., Coasne, B., Dufreche, J. F., Turq, P. Hydrophobic Transition in Porous Amorphous Silica. *J Phys Chem B* **2011**, *115*, 7881-7886.
20 Zhu, H., Ghoufi, A., Szymczyk, A., Balannec, B., Morineau, D. Anomalous Dielectric Behavior of Nanoconfined Electrolytic Solutions. *Phys. Rev. Lett.* **2012**, *109*, 107801.
21 Renou, R., Ghoufi, A., Szymczyk, A., Zhu, H., Neyt, J. C., Malfreyt, P. Nanoconfined Electrolyte Solutions in Porous Hydrophilic Silica Membranes. *J. Phys. Chem. C* **2013**, *117*, 11017-11027.
22 Dove, P. M., Craven, C. M. Surface Charge Density on Silica in Alkali and Alkaline Earth Chloride Electrolyte Solutions. *Geochim. Cosmochim. Acta* **2005**, *69*, 4963-4970.
23 Lowe, B. M., Skylaris, C. K., Green, N. G. Acid-Base Dissociation Mechanisms and Energetics at the Silica-Water Interface: An Activationless Process. *J. Colloid Interface Sci.* **2015**, *451*, 231-244.

24 Azam, M. S., Weeraman, C. N., Gibbs-Davis, J. M. Specific Cation Effects on the Bimodal Acid-Base Behavior of the Silica/Water Interface. *J. Phys. Chem. Lett* **2012**, *3*, 1269-1274.
25 Leung, K., Nielsen, I. M. B., Criscenti, L. J. Elucidating the Bimodal Acid-Base Behavior of the Water-Silica Interface from First Principles. *J. Am. Chem. Soc.* **2009**, *131*, 18359-18365.
26 Leroy, P., Maineult, A. Exploring the Electrical Potential inside Cylinders Beyond the Debye-Hückel Approximation: A Computer Code to Solve the Poisson-Boltzmann Equation for Multivalent Electrolytes. *Geophysical Journal International* **2018**.
27 Lyklema, J., Duval, J. F. Hetero-Interaction between Gouy-Stern Double Layers: Charge and Potential Regulation. *Adv Colloid Interface Sci* **2005**, *114-115*, 27-45.
28 Bonnaud, P. A., Coasne, B., Pellenq, R. J. Solvated Calcium Ions in Charged Silica Nanopores. *J. Chem. Phys.* **2012**, *137*, 064706.
29 Renou, R., Szymczyk, A., Ghoufi, A. Water Confinement in Nanoporous Silica Materials. *J. Chem. Phys.* **2014**, *140*, 044704.
30 Hartkamp, R., Siboulet, B., Dufreche, J. F., Coasne, B. Ion-Specific Adsorption and Electroosmosis in Charged Amorphous Porous Silica. *Phys. Chem. Chem. Phys.* **2015**, *17*, 24683-24695.
31 Haria, N. R., Lorenz, C. D. Atomistic Description of Pressure-Driven Flow of Aqueous Salt Solutions through Charged Silica Nanopores. *J. Phys. Chem. C* **2015**, *119*, 12298-12311.
32 Haria, N. R., Lorenz, C. D. Ion Exclusion and Electrokinetic Effects Resulting from Electro-Osmotic Flow of Salt Solutions in Charged Silica Nanopores. *Phys. Chem. Chem. Phys.* **2012**, *14*, 5935-5944.
33 Teppen, B. J., Miller, D. M. Hydration Energy Determines Isovalent Cation Exchange Selectivity by Clay Minerals. *Soil Sci. Soc. Am. J.* **2006**, *70*, 31.
34 Quintas, A., Charpentier, T., Majerus, O., Caurant, D., Dussossoy, J. L., Vermaut, P. Nmr Study of a Rare-Earth Aluminoborosilicate Glass with Varying Cao-to-Na_2o Ratio. *Appl. Magn. Reson.* **2007**, *32*, 613-634.
35 Eberl, D. D. Alkali Cation Selectivity and Fixation by Clay Minerals. *Clays Clay Miner.* **1980**, *28*, 161-172.
36 Cruz-Chu, E. R., Aksimentiev, A., Schulten, K. Water-Silica Force Fiel for Simulating Nanodevices. *J. Phys. Chem. B* **2006**, *110*, 21497-21508.
37 Ohno, H., Kahara, S., Umesake, N., Suzuya, K. High-Energy X-Ray Diffraction Studies of Non-Crystalline Materials. *J. Non Cryst. Solids* **2001**, *293-295*, 125-135.
38 Cygan, R. T., Liang, J.-J., Kalinichev, A. G. Molecular Models of Hydroxide, Oxyhydroxide, and Clay Phases and the Development of a General Force Field. *J. Phys. Chem. B* **2004**, *108*, 1255-1266.
39 Berendsen, H. J. C., Grigera, J. R., Straatsma, T. P. The Missing Term in Effective Pair Potentials. *J. Phys. Chem.* **1987**, *91*, 6269-6271.
40 Smith, D. E., Dang, L. X. Computer Simulations of Nacl Association in Polarizable Water. *J. Chem. Phys.* **1994**, *100*, 3757-3766.
41 Dang, L. X. Development of Nonadditive Intermolecular Potentials Using Molecular Dynamics: Solvation of Li^+ and F^- Ions in Polarizable Water. *J. Chem. Phys.* **1992**, *96*, 6970-6977.
42 Dang, L. X. Mechanism and Thermodynamics of Ion Selectivity in Aqueous Solutions of 18-Crown-6 Ether: A Molecular Dynamics Study. *J. Am. Chem. Soc.* **1995**, *117*, 6954-6960.
43 Wasserman, E., Wood, B., Brodholt, J. The Static Dielectric Constant of Water at Pressures up to 20 Kbar and Temperatures to 1273 K: Experiment, Simulations, and Empirical Equations. *Geochim. Cosmochim. Acta* **1994**, *59*, 1-6.
44 Hura, G., Russo, D., Glaeser, R. M., Head-Gordon, T., Krack, M., Parrinello, M. Water Structure as a Function of Temperature from X-Ray Scattering Experiments and Ab Initio Molecular Dynamics. *Phys. Chem. Chem. Phys.* **2003**, *5*, 1981.

45 Skelton, A. A., Fenter, P., Kubicki, J. D., Wesolowski, D. J., Cummings, P. T. Simulations of the Quartz(10$\bar{1}$1)/Water Interface: A Comparison of Classical Force Fields, Ab Initio Molecular Dynamics, and X-Ray Reflectivity Experiments. *J. Phys. Chem. C* **2011**, *115*, 2076-2088.
46 Bourg, I., Sposito, G. Connecting the Molecular Scale to the Continuum Scale for Diffusion Processes in Smectite-Rich Porous Media. *Environ. Sci. Technol.* **2010**, *44*, 2085-2091.
47 Ferrage, E., Sakharov, B. A., Michot, L. J., Delville, A., Bauer, A., Lanson, B., Grangeon, S., Frapper, G., Jiménez-Ruiz, M., Cuello, G. J. Hydration Properties and Interlayer Organization of Water and Ions in Synthetic Na-Smectite with Tetrahedral Layer Charge. Part 2. Toward a Precise Coupling between Molecular Simulations and Diffraction Data. *J. Phys. Chem. C* **2011**, *115*, 1867-1881.
48 Bourg, I. C., Lee, S. S., Fenter, P., Tournassat, C. Stern Layer Structure and Energetics at Mica–Water Interfaces. *J. Phys. Chem. C* **2017**, *121*, 9402-9412.
49 Lammers, L. N., Bourg, I. C., Okumura, M., Kolluri, K., Sposito, G., Machida, M. Molecular Dynamics Simulations of Cesium Adsorption on Illite Nanoparticles. *J. Colloid Interface Sci.* **2017**, *490*, 608-620.
50 Kerisit, S., Liu, C. Molecular Simulations of Water and Ion Diffusion in Nanosized Mineral Fractures. *Environ. Sci. Technol.* **2009**, *43*, 777-782.
51 Predota, M., Bandura, A. V., Cummings, P. T., Kubicki, J. D., Wesolowski, D. J., Chialvo, A. A., Machesky, M. L. Electric Double Layer at the Rutile (110) Surface. 1. Structure of Surfaces and Interfacial Water from Molecular Dynamics by Use of Ab Initio Potentials. *J. Phys. Chem. B* **2004**, *108*, 12049-12060.
52 Lorenz, C. D. Molecular Dynamics of Ionic Transport and Electrokinetic Effects in Realistic Silica Channels. *J. Phys. Chem. C* **2008**, *112*, 10222-10232.
53 Plimpton, S. Fast Parallel Algorithms for Short–Range Molecular Dynamics. *J. Comput. Phys.* **1995**, *117*, 1-19.
54 Humphrey, W., Dalke, A., Schulten, K. Vmd: Visual Molecular Dynamics. *J. Mol. Graph.* **1996**, *14*, 33-38.
55 Lockwood, G. K., Garofalini, S. H. Lifetimes of Excess Protons in Water Using a Dissociative Water Potential. *J. Phys. Chem. B* **2013**, *117*, 4089-4097.
56 Mahadevan, T., Garofalini, S. Dissociative Chemisorption of Water onto Silica Surfaces and Formation of Hydronium Ions (Vol 112c, Pg 1507, 2008). *J. Phys. Chem. C* **2009**, *113*, 11177-11177.
57 Mahadevan, T. S., Garofalini, S. Dissociative Water Potentialfor Molecular Dynamics Simulations. *J. Phys. Chem. B* **2007**, *111*, 8919-8927.
58 Crank, J. *The Mathematics of Diffusion*. New York, 1975.
59 Dazas, B., Lanson, B., Delville, A., Robert, J.-L., Komarneni, S., Michot, L. J., Ferrage, E. Influence of Tetrahedral Layer Charge on the Organization of Interlayer Water and Ions in Synthetic Na-Saturated Smectites. *J. Phys. Chem. C* **2015**, *119*, 4158-4172.
60 Pfeiffer-Laplaud, M., Gaigeot, M.-P. Adsorption of Singly Charged Ions at the Hydroxylated (0001) A-Quartz/Water Interface. *J. Phys. Chem. C* **2016**, *120*, 4866-4880.
61 Boda, D., Valisko, M., Henderson, D., Gillespie, D., Eisenberg, B., Gilson, M. K. Ions and Inhibitors in the Binding Site of Hiv Protease: Comparison of Monte Carlo Simulations and the Linearized Poisson-Boltzmann Theory. *Biophys. J.* **2009**, *96*, 1293-1306.
62 Tournassat, C., Bourg, I., Holmboe, M., Sposito, G., Steefel, C. Molecular Dynamics Simulations of Anion Exclusion in Clay Interlayer Nanopores. *Clays Clay Miner.* **2016**, *64*, 374-388.
63 Hocine, S., Hartkamp, R., Siboulet, B., Duvail, M., Coasne, B., Turq, P., Dufrêche, J.-F. How Ion Condensation Occurs at a Charged Surface: A Molecular Dynamics Investigation of the Stern Layer for Water–Silica Interfaces. *J. Phys. Chem. C* **2016**, *120*, 963-973.

64 Salles, F., Bildstein, O., Douillard, J. M., Jullien, M., Van Damme, H. Determination of the Driving Force for the Hydration of the Swelling Clays from Computation of the Hydration Energy of the Interlayer Cations and the Clay Layer. *J. Phys. Chem. C* **2007**, *111*, 13170-13176.
65 Kuyucak, S., Andersen, O. S., Chung, S. Models of Permeation in Ion Channels. *Rep. Prog. Phys.* **2001**, *64*, 1427-1472.
66 Sverjensky, D. A., Sahai, N. Theoretical Prediction of Single Site Protonation Equilibrium Constants for Oxides and Silicates in Water. *Geochim. Cosmochim. Acta* **1996**, *60*, 3773-3797.
67 Mamontov, E., Cole, D. R. Quasielastic Neutron Scattering Study of Dynamics of Cacl2 Aqueous Solution Confined in Vycor Glass. *Phys. Chem. Chem. Phys.* **2006**, *8*, 4908-4914.
68 Garofalini, S. H., Mahadevan, T. S., Xu, S., Scherer, G. W. Molecular Mechanisms Causing Anomalously High Thermal Expansion of Nanoconfined Water. *Chemphyschem* **2008**, *9*, 1997-2001.
69 Gallo, P., Ricci, M. A., Rovere, M. Layer Analysis of the Structure of Water Confined in Vycor Glass. *J. Chem. Phys.* **2002**, *116*, 342.
70 Lee, S. H., Rossky, P. J. A Comparison of the Structure and Dynamics of Liquid Water at Hydrophobic and Hydrophilic Surfaces—a Molecular Dynamics Simulation Study. *J. Chem. Phys.* **1994**, *100*, 3334-3345.
71 Spohr, E., Hartnig, C. Water in Porous Glasses. A Computer Simulation Study. *J. Mol. Liq.* **1999**, *80*, 165-178.
72 Gallo, P., Rapinesi, M., Rovere, M. Confined Water in the Low Hydration Regime. *J. Chem. Phys.* **2002**, *117*, 369-375.

TOC Graphic